





## Mesomorphism of novel stilbene-based bent-core liquid crystals

N. Trišović, L. Matović, T. Tóth-Katona, R. Saha & A. Jákli


To cite this article: N. Trišović, L. Matović, T. Tóth-Katona, R. Saha & A. Jákli (2021) Mesomorphism of novel stilbene-based bent-core liquid crystals, *Liquid Crystals*, 48:7, 1054-1064, DOI: [10.1080/02678292.2020.1839800](https://doi.org/10.1080/02678292.2020.1839800)

To link to this article: <https://doi.org/10.1080/02678292.2020.1839800>

 View supplementary material 

 Published online: 28 Dec 2020.

 Submit your article to this journal 

 Article views: 181

 View related articles 

 View Crossmark data 



## Mesomorphism of novel stilbene-based bent-core liquid crystals

N. Trišović<sup>a</sup>, L. Matović<sup>b</sup>, T. Tóth-Katona<sup>c</sup>, R. Saha<sup>d</sup> and A. Jáklí<sup>c,d,e</sup>

<sup>a</sup>Faculty of Technology and Metallurgy, University of Belgrade, Belgrade, Serbia; <sup>b</sup>Innovation Centre of the Faculty of Technology and Metallurgy, Belgrade, Serbia; <sup>c</sup>Institute for Solid State Physics and Optics, Wigner Research Centre for Physics, Budapest, Hungary; <sup>d</sup>Department of Physics, Kent State University, Kent, OH, USA; <sup>e</sup>Chemical Physics Interdisciplinary Program, Advanced Materials and Liquid Crystal Institute, Kent State University, Kent, OH, USA

### ABSTRACT

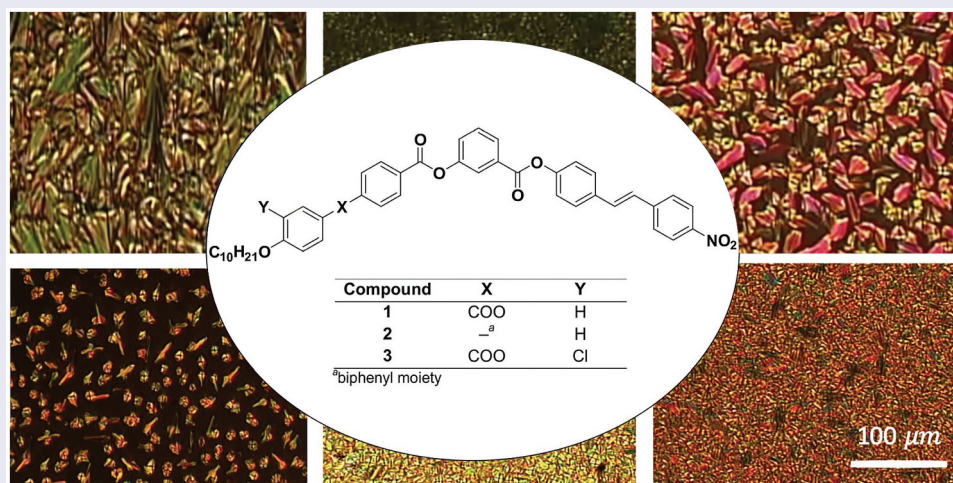
A series of asymmetric bent-core liquid crystals, bearing the stilbene moiety in the side wing, was synthesised and characterised. Structural modifications of the non-stilbene wing resulted in formation of various mesophases. Compounds **1** and **3** with an ester linking group between the phenyl rings in this wing have an enantiotropic non-polar smectic-type mesophase, while compound **2**, incorporating the biphenyl moiety, has a ferroelectric  $\text{SmC}_a\text{P}_F$  phase. The molecules of **2** undergo photoisomerisation in solution under UV irradiation, while the mesophases are unstable and UV irradiation leads to irreversible changes. The mesophases of **1** and **3** do not show any electro-optical switching and polarisation current. Applying low frequency AC voltage on a planarly aligned film of compound **2**, smectic domains grow, while the birefringence and an image flickering increase. The observed features of these compounds identify stilbene as an attractive moiety in the design of advanced materials based on bent-core molecules.

### ARTICLE HISTORY

Received 6 August 2020  
Accepted 17 October 2020

### KEYWORDS

Bent-core liquid crystals; stilbene; photoresponsive materials; structure–property relationship




## 1. Introduction

Designing a chemical system that undergoes several tuning processes is particularly important in development of new stimuli responsive materials [1–4]. Conformational changes of the individual structural fragments in these materials can produce drastic transformations in their macroscopic properties in response to an applied external stimulus. So far, a wide variety of property control and activation mechanism has been proposed. Among them light has been recognised as the most attractive stimulus. Recent developments have been focusing on photo-

responsive self-assembled supramolecular architectures, such as azobenzene-based liquid crystals (LCs) [5,6]. In these systems, the assembled molecules have considerable rotational freedom and the conversion from the more stable *trans*-isomer to the less stable *cis*-isomer may lead to mesophase transition upon light irradiation. Such transitions enable promising applications in the areas of optical data storage and dynamic holography [7–9].

Other photochromic moieties have also been used to achieve the photo-control of LC systems. Stilbene and its derivatives offer facile synthesis and structural

**CONTACT** N. Trišović ✉ [ntrisovic@tmf.bg.ac.rs](mailto:ntrisovic@tmf.bg.ac.rs)

 Supplemental data for this article can be accessed [here](#).

© 2020 Informa UK Limited, trading as Taylor & Francis Group

tunability, interesting photophysical and photochemical properties which make this moiety attractive to design self-assembled supramolecular architectures [10–12]. Due to the *trans*-to-*cis* photoisomerisation ability, it can influence the polarity and the structure within the materials upon light irradiation in a reversible manner [13]. Several stilbene derivatives with various chiral auxiliaries were reported in order to tune the helical twisting power of cholesteric LC hosts upon light irradiation [14]. It was demonstrated that the photoinduced structure transfer from stilbenes onto an LC phase of the host is 7–8 times larger than for the structurally related azobenzene guests [15]. Ichimura and co-workers even performed surface-assisted LC photoalignment by fabricating LC cells with substrates modified with photochromic stilbene-based molecules [16,17].

Stilbene and its derivatives were incorporated into LC molecules of different shapes. It was demonstrated that 4,4'-dialkoxy-*trans*-stilbenes exhibited nematic mesophases at higher temperatures [18]. Steric crowding of different substituents about the double bond resulted in an increase in the melting points of nonplanar stilbenes in comparison to their planar counterparts. Within a series of mono- and dimethyl-substituted *trans*-stilbenes, a relationship between the increase in molecular breadth and the lowering of the stability of the nematic phase was also found. Although twisting the stilbene out of planarity appeared to produce a decrease of the clearing point, the intermolecular separation was recognised as the prevailing feature [19]. Fouquey *et al.* reported that the highly polarisable rod-like push-pull stilbene derivatives exhibited only an SmA and/or SmE phases [20], while terminally substituted stilbene-toluene LCs had a wide nematic range, although the increased conjugation causes the increased rigidity and higher transition temperatures [21]. In the search for new reactive LCs bearing crosslinkable functional groups, Ou *et al.* synthesised mono- and di-cyanates with *trans*-stilbene structure, where appropriate curing process resulted in discogens exhibiting nematic phase at higher temperatures [22]. A fusion of two photochromic moieties (azobenzene and stilbene) in a rod-like LC dimer provided interesting properties, including a wide smectic range, sensitivity to the light from both UV and visible range and luminescence in the visible area [23]. Lehmann and co-workers investigated stilbenoid shape-persistent star-shaped LCs, which pack densely in a columnar helical arrangement [24–26]. A particular feature of these dendrimers is the existence of intrinsic empty space where guest molecules can be incorporated. Adjusting the conjugated arms and the size of this space to selected functional guests enables the formation of LCs with more than one building block where the stilbenoid moieties

and chromophores, e.g. anthracene derivatives or fullerene, are double nanosegregated side-by-side in a single column. Gupta *et al.* reported that enhanced intermolecular interactions in star-shaped tris(*N*-salicylideneanilines) bearing the cyanostilbene moiety stabilised Col<sub>r</sub> phase in comparison to the columnar hexagonal phase of stilbene derivative, thus exhibiting the freezing of this phase into glassy state [27].

Bent-core LCs have attracted considerable attention in recent years due to their rich and unusual mesomorphism, supramolecular chirality as well as significant ferroelectric and antiferroelectric properties. Unlike for rod-like LCs, it has been difficult to predict the mesophase temperature range of these compounds. This is due to the subtle balance between order and disorder. Martínez-Abadía *et al.* reported several bent-core molecules with one or two cyanostilbene units in the side wings and different position of the cyano group exhibiting a variety of mesophases (columnar, polar smectic and dark conglomerate phases) [28–30]. The mesophase formation offered the possibility to explore how sensitive this chromophore is on different molecular arrangements in these materials.

Here, we report the synthesis and physical characterisation of a series of asymmetric bent-core LCs incorporating 4-nitrostilbene moiety in the side wing, where the nitro group located in para position of the aromatic ring broadens the  $\pi$ -conjugation within the molecules (Figure 1). To the best of our knowledge, this moiety has not been used in the design of bent-core LCs before. We find that a combination of LC properties and photosensitivity enables these compounds to become a bridge from functional  $\pi$ -conjugated systems to materials for advanced technological applications.

## 2. Experimental methods

### 2.1 Materials and methods

Unless otherwise stated, all starting materials, reagents and solvents were obtained from commercial suppliers and used without further purification. The synthetic route to the investigated compounds is presented in Schemes 1 and 2. Compounds 4–8 were prepared according to procedures from the literature [31–35]. Because their characterisation data are in agreement with those previously reported, experimental details are not included here. A detailed description of the synthesis of representative intermediates and the investigated compounds and the structural characterisation of the latter are presented in this work. The structural characterisation of benzoic acid derivatives (9) is given in Supplementary information.

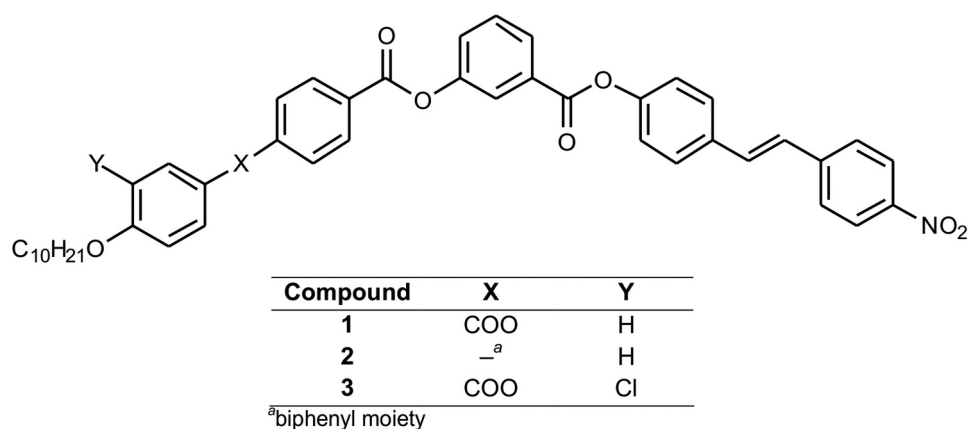
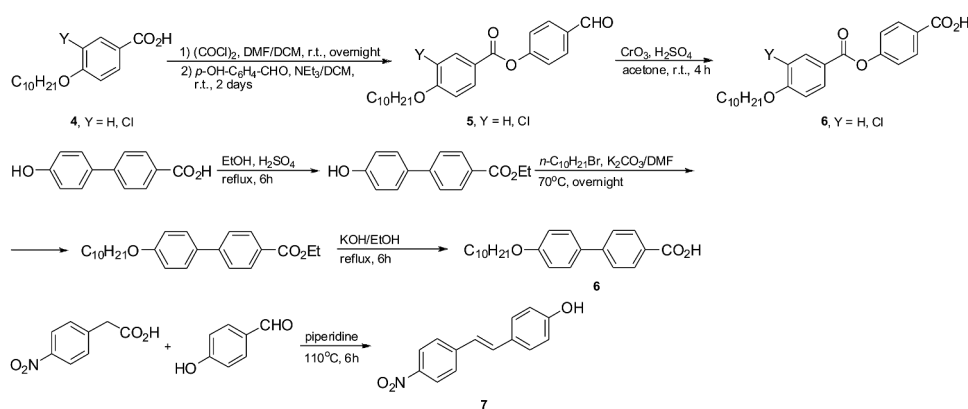
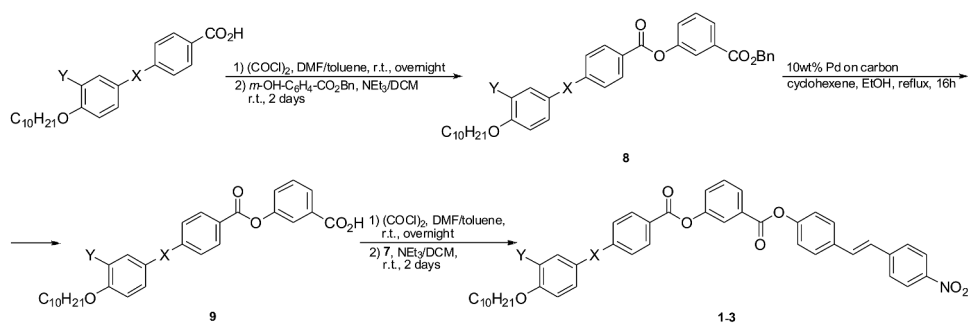


Figure 1. Chemical structures of the investigated bent-core molecules.



Scheme 1. Synthesis of building blocks used as the wings in the investigated bent-core molecules.



Scheme 2. Synthesis of the investigated compounds (1–3).

The FTIR spectra of the synthesised compounds were recorded with a Bomem MB series 100 spectrophotometer using the KBr pellets. The NMR spectral measurements were performed on a Bruker 300 spectrometer at 400 MHz for the  $^1\text{H}$  NMR and 100 MHz for the  $^{13}\text{C}$  NMR spectra. The spectra were recorded at room temperature in  $\text{DMSO}-d_6$  or  $\text{CDCl}_3$  using TMS as the internal standard. The elemental analysis of the synthesised compounds was carried out by standard analytical micromethods using an Elemental

Vario EL III microanalyzer. Their results were found to be in good agreement ( $\pm 0.3\%$ ) with the calculated values.

### 2.1.1 General procedure for the synthesis of acids (9)

Benzyl ester **8** (5.0 mmol) was suspended in ethanol (150 ml) and cyclohexene (75 ml) and 10 wt% Pd on carbon (0.40 g) was added. The mixture was heated under reflux and the reaction was followed by TLC. After 16 hours, the mixture was filtered off and the



filtrate was evaporated to give a white solid. The obtained compound was purified by recrystallisation from acetic acid.

### 2.1.2 General procedure for synthesis of the investigated compounds (1–3)

To a suspension of acid **9** (2.5 mmol) and oxalyl chloride (1.10 ml, 12.5 mmol) in dry toluene (50 ml) a drop of dimethylformamide was added and the mixture was stirred at room temperature until the suspension cleared out. After volatiles had been removed under vacuum, the residue was dissolved in dry dichloromethane (40 ml) and the solution was added to a solution of 4-nitro-4'-hydroxystilbene (**7**, 0.60 g, 2.5 mmol) and trimethylamine (0.38 ml, 2.75 mmol) in dry dichloromethane (40 ml). The reaction was stirred at room temperature for 2 days. The reaction mixture was washed with 5% aqueous solution of HCl and brine successively, dried over MgSO<sub>4</sub> and then concentrated. The obtained yellow solid was purified by column chromatography using chloroform as eluent and further recrystallised from a toluene/hexane mixture.

#### 2.1.2.1. 4'-Nitro-4-stilbenyl 3-(((4-(4-decyloxybenzoyl)oxy)benzoyl)oxy)benzoate (1)

Yield: 68%; FTIR (KBr): 2937, 2921, 2851, 1750, 1738, 1605, 1591, 15,010, 1467, 1442, 1336, 1309, 1252, 1199, 1160, 1109, 913, 852, 760, 746 cm<sup>-1</sup>; <sup>1</sup>H NMR (400 MHz, CDCl<sub>3</sub>): 0.82 (t, 3 H, *J* = 6.2 Hz, -CH<sub>3</sub>), 1.15–1.35 (m, 12 H, -CH<sub>2</sub>-), 1.41 (quin, 2 H, *J* = 7.3 Hz, -CH<sub>2</sub>-), 1.76 (quin, 2 H, *J* = 7.2 Hz, -CH<sub>2</sub>-), 3.98 (t, 2 H, *J* = 6.6 Hz, -CH<sub>2</sub>O-), 6.92 (d, 2 H, *J* = 8.8 Hz, -C<sub>6</sub>H<sub>4</sub>-), 7.05 (d, 1H, *J* = 16.6 Hz, -CH<sub>2</sub> = CH<sub>2</sub>-), 7.20 (d, 2 H, *J* = 9.2 Hz, -C<sub>6</sub>H<sub>4</sub>-), 7.21 (d, 1H, *J* = 16.6 Hz, -CH<sub>2</sub> = CH<sub>2</sub>-), 7.32 (d, 2 H, *J* = 8.8 Hz, -C<sub>6</sub>H<sub>4</sub>-), 7.43–7.50 (m, 1H), 7.53 (d, 1H, *J* = 7.2 Hz, -C<sub>6</sub>H<sub>4</sub>-), 7.54 (d, 2 H, *J* = 9.2 Hz, -C<sub>6</sub>H<sub>4</sub>-), 7.57 (d, 2 H, *J* = 9.2 Hz, -C<sub>6</sub>H<sub>4</sub>-), 8.00 (s, 1H, -C<sub>6</sub>H<sub>4</sub>-), 7.98–8.11 (m, 3 H, -C<sub>6</sub>H<sub>4</sub>-), 8.15 (d, 2 H, *J* = 8.8 Hz, -C<sub>6</sub>H<sub>4</sub>-), 8.23 (d, 2 H, *J* = 8.8 Hz, -C<sub>6</sub>H<sub>4</sub>-) ppm; <sup>13</sup>C NMR (100 MHz, CDCl<sub>3</sub>): 14.1, 22.7, 26.0, 29.1, 29.3, 29.4, 29.6, 31.9, 68.4, 114.5, 120.9, 122.1, 122.2, 122.3, 123.6, 124.2, 126.4, 126.6, 126.9, 127.3, 127.8, 128.1, 129.8, 131.0, 131.9, 132.3, 132.4, 134.2, 143.7, 146.9, 151.0, 151.1, 155.7, 163.9, 164.1, 164.3 ppm; Elemental analysis: for C<sub>45</sub>H<sub>43</sub>NO<sub>9</sub>: calculated C 72.86, H 5.84, N 1.89; found: C 72.79, H 5.85, N 1.97%.

#### 2.1.2.2. 4'-Nitro-4-stilbenyl 3-(4'-decyloxybiphenyl-4-carbonyloxy)benzoate (2)

Yield: 72%; FTIR (KBr): 2919, 2850, 1734, 1604, 1593, 1509, 1467, 1442, 1341, 1254, 1194, 1107, 1078, 914, 832, 800, 765, 751, 731, 692 cm<sup>-1</sup>; <sup>1</sup>H NMR (400 MHz,

CDCl<sub>3</sub>): 0.91 (t, 3 H, *J* = 6.6 Hz, -CH<sub>3</sub>), 1.28–1.41 (m, 12 H, -CH<sub>2</sub>-), 1.51 (quin, 2 H, *J* = 7.3 Hz, -CH<sub>2</sub>-), 1.85 (quin, 2 H, *J* = 7.2 Hz, -CH<sub>2</sub>-), 4.05 (t, 2 H, *J* = 6.6 Hz, -CH<sub>2</sub>O-), 7.04 (d, 2 H, *J* = 8.4 Hz, -C<sub>6</sub>H<sub>4</sub>-), 7.15 (d, 1H, *J* = 16 Hz, -CH<sub>2</sub> = CH<sub>2</sub>-), 7.30 (d, 2 H, *J* = 8.4 Hz, -C<sub>6</sub>H<sub>4</sub>-), 7.30 (d, 1H, *J* = 16.8 Hz, -CH<sub>2</sub> = CH<sub>2</sub>-), 7.55–7.59 (m, 1H, -C<sub>6</sub>H<sub>4</sub>-), 7.62–7.70 (m, 7 H, -C<sub>6</sub>H<sub>4</sub>-), 7.74 (d, 2 H, *J* = 8 Hz, -C<sub>6</sub>H<sub>4</sub>-), 8.11 (s, 1H, -C<sub>6</sub>H<sub>4</sub>-), 8.17 (d, 1H, *J* = 7.6 Hz, -C<sub>6</sub>H<sub>4</sub>-), 8.26 (d, 2 H, *J* = 10 Hz, -C<sub>6</sub>H<sub>4</sub>-), 8.28 (d, 2 H, *J* = 8.8 Hz, -C<sub>6</sub>H<sub>4</sub>-) ppm; <sup>13</sup>C NMR (100 MHz, CDCl<sub>3</sub>): 14.1, 22.7, 26.1, 29.2, 29.3, 29.4, 29.5, 29.6, 31.9, 68.2, 115.1, 122.2, 123.7, 124.2, 126.6, 126.7, 126.9, 127.0, 127.4, 127.7, 128.1, 128.4, 129.8, 130.8, 131.0, 131.8, 132.2, 134.2, 143.7, 146.9, 151.1, 151.2, 159.7, 164.2, 165.0 ppm; Elemental analysis: for C<sub>44</sub>H<sub>43</sub>NO<sub>7</sub>: calculated C 75.73, H 6.21, N 2.01; found: C 75.76, H 6.14, N 2.05%.

#### 2.1.2.3. 4'-Nitro-4-stilbenyl 3-(((4-(3-chloro-4-decyloxybenzoyl)oxy)benzoyl)oxy)benzoate (3)

Yield: 60%; FTIR (KBr): 2953, 2923, 2854, 1736, 15,967, 1508, 1468, 1446, 1412, 1343, 1277, 1259, 1232, 1211, 1164, 1067, 1108, 899, 848, 754, 685 cm<sup>-1</sup>; <sup>1</sup>H NMR (400 MHz, CDCl<sub>3</sub>): 0.82 (t, 3 H, *J* = 6.6 Hz, -CH<sub>3</sub>), 1.20–1.37 (m, 12 H, -CH<sub>2</sub>-), 1.45 (quin, 2 H, *J* = 7.4 Hz, -CH<sub>2</sub>-), 1.82 (quin, 2 H, *J* = 7.2 Hz, -CH<sub>2</sub>-), 4.06 (t, 2 H, *J* = 6.4 Hz, -CH<sub>2</sub>O-), 6.94 (d, 2 H, *J* = 8.8 Hz, -C<sub>6</sub>H<sub>3</sub>-), 7.06 (d, 1H, *J* = 16.4 Hz, -CH<sub>2</sub> = CH<sub>2</sub>-), 7.20 (d, 2 H, *J* = 8.8 Hz, -C<sub>6</sub>H<sub>4</sub>-), 7.21 (d, 1H, *J* = 17.0 Hz, -CH<sub>2</sub> = CH<sub>2</sub>-), 7.32 (d, 2 H, *J* = 8.4 Hz, -C<sub>6</sub>H<sub>4</sub>-), 7.43–7.50 (m, 1H, -C<sub>6</sub>H<sub>4</sub>-), 7.51–7.60 (m, 4H, -C<sub>6</sub>H<sub>4</sub>- and -C<sub>6</sub>H<sub>3</sub>-), 8.04 (s, 1H, -C<sub>6</sub>H<sub>4</sub>-), 8.06 (d, 2 H, *J* = 8.0 Hz, -C<sub>6</sub>H<sub>4</sub>-), 8.07 (d, 1H, *J* = 8.0 Hz, -C<sub>6</sub>H<sub>4</sub>-), 8.13–8.19 (m, 2 H, -C<sub>6</sub>H<sub>3</sub>-), 8.24 (d, 2 H, *J* = 8.8 Hz, -C<sub>6</sub>H<sub>4</sub>-) ppm; <sup>13</sup>C NMR (100 MHz, CDCl<sub>3</sub>): 14.1, 22.7, 25.9, 28.9, 29.2, 29.3, 29.5, 31.9, 69.5, 112.3, 121.9, 122.1, 122.2, 123.3, 123.6, 123.7, 124.2, 126.6, 126.7, 126.9, 127.3, 127.8, 128.1, 129.7, 129.8, 130.0, 130.7, 131.0, 132.0, 132.2, 132.3, 132.9, 134.2, 143.7, 146.9, 151.0, 151.1, 155.4, 159.2, 163.4, 164.1, 164.2 ppm; Elemental analysis: for C<sub>45</sub>H<sub>42</sub>ClNO<sub>9</sub>: calculated C 69.63, H 5.45, N 1.80; found: C 69.60, H 5.48, N 1.81%.

## 2.2 Polarising optical microscopy

The POM textures of all materials were investigated using Olympus BX60 polarising microscope by placing 5 μm liquid crystal sandwich cells with planar alignment in Instec HS2000 heat stage. The POM textures were studied while heating at 2°C/min, and cooling the sample from the isotropic phase through all the liquid crystal phases with 1°C/min rate.

### 2.3 Small angle X-ray scattering

SAXS measurements were done in beamline 7.3.3 of the Advanced Light Source (ALS) at Lawrence Berkeley Laboratory in USA. The sample was loaded into 1.5 mm glass capillary tubes and placed on a customised hot stage. To align our sample, we applied an external magnetic field of about 1.5 T with the capillary situated between the magnets. The sample was heated into the isotropic phase and cooled to remove any defects.

### 2.4 UV-Vis spectroscopy

UV-Vis spectroscopy investigations were performed in SHIMADZU UV-3600 plus UV-VIS-NIR spectrometer. For irradiation experiment, we used the dichloromethane solution of the materials ( $3 \times 10^{-4}$  M) filled in quartz tube at room temperature and irradiated by 365 nm UV with  $1 \text{ mW/cm}^2$  intensity.

### 2.5 Electro-optical observations

Electro-optical experiments were carried out on 5  $\mu\text{m}$  thick cell in which compound **2** was sandwiched between transparent indium tin oxide (ITO) electrodes and antiparallel rubbed polyimide alignment layers. The sandwich cells were placed in Instec., HS2000 heat stage and viewed through Olympus BX60 polarising microscope equipped with crossed polarisers. The electric signals were applied by a HP 33120A function generator and amplified by FLC E20AD voltage amplifier. The signals of a photodiode placed in the eyepiece of the microscope were inputted on to an InfiniVision MSO-X 302A mixed signal oscilloscope.

### 2.6 Differential scanning calorimetry

The DSC plots for all compounds directly taken from the Perkin Elmer Pyris 1 instrument. The samples were obtained directly from recrystallisation and measured at  $10^\circ\text{C}/\text{min}$  heating and cooling rates.

## 3. Results and discussion

### 3.1 Synthesis

The structure with five aromatic rings was constructed by a stepwise acylation of 3-hydroxybenzoic acid as the central unit, analogously as reported in the literature (Schemes 1 and 2) [31]. Namely, the synthesis of compounds **1** and **3** started from the reaction between 3-substituted 4-decyloxybenzoyl chloride and 4-hydroxybenzaldehyde followed by an oxidation of compound **5** to obtain 4-(3-substituted

4-decyloxybenzoyloxy) benzoic acid (**6**). This acid (or 4-decyloxybiphenylcarboxylic acid in the case of synthesis of compound **2**) was further converted to chloride and attached to benzyl 3-hydroxybenzoate giving intermediate **8**, deprotection of which gave the intermediate **9**. Finally, the esterification of this compound with compound **7**, which was previously obtained by a condensation reaction between 4-nitrophenylacetic acid and 4-hydroxybenzaldehyde, afforded compounds **1–3**.

### 3.2 Characterisation

The mesomorphic behaviour of compounds **1–3** was initially studied by polarised optical microscopy (POM), electro-optical switching and polarisation current. Further studies by means of small angle X-ray scattering (SAXS), and detailed photoisomerisation measurements are presented only on compound **2**, which has the most interesting mesophases. The UV-Vis spectra taken after different illumination times are also given for all compounds in dichloromethane solutions.

#### 3.2.1 Polarising optical microscopy

Figure 2 shows the polarised optical microscopy (POM) textures of 5  $\mu\text{m}$  cells with planar alignment after cooling from the isotropic phase at  $1^\circ\text{C}/\text{min}$  rate. Figure 2(a-d) shows the textures of compounds **1**, **2** and **3**, respectively. The fan-shaped domains seen in (a) at  $135^\circ\text{C}$  of compound **1** are characteristic to a smectic phase. The elongated domains appear dark when their long axis is making about  $15\text{--}20^\circ$ , suggesting tilted (SmC) smectic phase. The elongated focal conic domains in Figure 2(b,c) for compound **2** at  $135^\circ\text{C}$  and  $105^\circ\text{C}$ , respectively, also indicate smectic phases. While the birefringence of the domains at  $135^\circ\text{C}$  is fairly uniform, the domains at  $105^\circ\text{C}$  are broken to smaller domains and have irregular birefringence colour. Figure 2(d) for compound **3** at  $110^\circ\text{C}$  show growing 'batonnets' into the isotropic phase, indicative of an isotropic fluid – smectic liquid crystal transition.

#### 3.2.2 Electro-optical observations

The mesophases of compounds **1** and **3** do not show any electro-optical switching and polarisation current peak up to  $10 \text{ V}/\mu\text{m}$  fields. Due to high ionic conductivity, upon increasing the field up to  $20 \text{ V}/\mu\text{m}$  at  $145^\circ\text{C}$  for **1** and  $110^\circ\text{C}$  for **3** we find the sample is heated to the isotropic phase (Figure 3(b,e)) and turning off a grainy texture forms due to fast cooling from the isotropic phase (Figure 3(c,f)). The elongated focal conics in the textures formed after slow cooling in zero field indicate

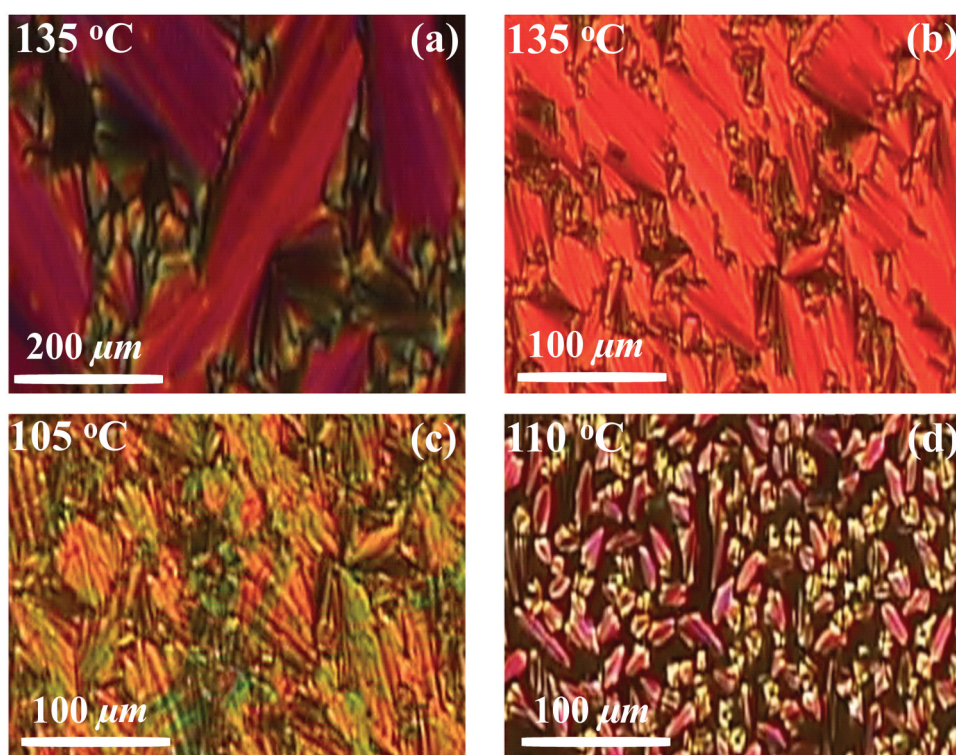


**Figure 2.** (Colour online) Polarising optical microscopy (POM) textures of compound **1**, **2** and **3** in 5  $\mu\text{m}$  thick planar cells. (a): Compound **1** at 135°C showing fan textures characteristic to a SmC phase; (b) and (c): the POM textures of compound **2** with fan shaped domain at 135°C and 105°C. (d) Growing 'batonnets' of compound **3** at 110°C.

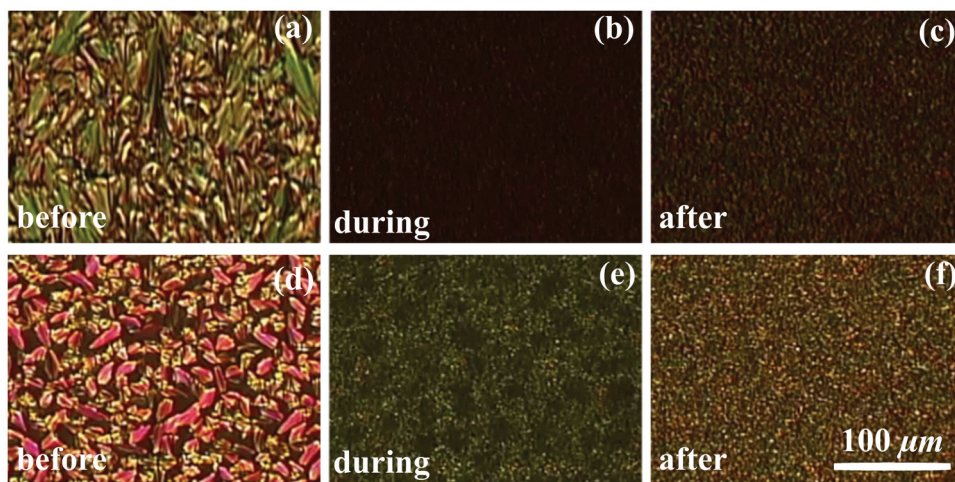


**Figure 3.** (Colour online) POM textures of 5  $\mu\text{m}$  thick planar aligned sandwich cells of materials **1** (upper row) and **3** (bottom row) at 145°C and 110°C, respectively. Left column (a,d): POM textures before application of any electric field. Middle column (b,e): POM textures during  $V_{p-p} = 80$  V,  $f = 12$  Hz rectangular voltage applied. Right column (c,f): POM texture 3 seconds after the voltage turned off.

smectic phase with optic axis slightly ( $\sim 15^\circ$ ) away from the long axis of the focal conic domains, which is parallel to the smectic layer normal.

Applying low-frequency AC voltage on 5  $\mu\text{m}$  thick planar aligned cell of compound **2**, we found a gradual growth of smectic domains and increase of the birefringence. Comparing the textures before any

voltage treatment (Figure 4(a)) and 3 minutes after 4  $\text{V}/\mu\text{m}$  amplitude 16 Hz square-wave voltage applied (Figure 4(b)) one sees the average size of the domains increased from about 10 to about 100  $\mu\text{m}$ . The increase of the domain size is likely due to the inhomogeneous director rotation during sign inversion of the applied voltage, which is coupled to flow (backflow). Such



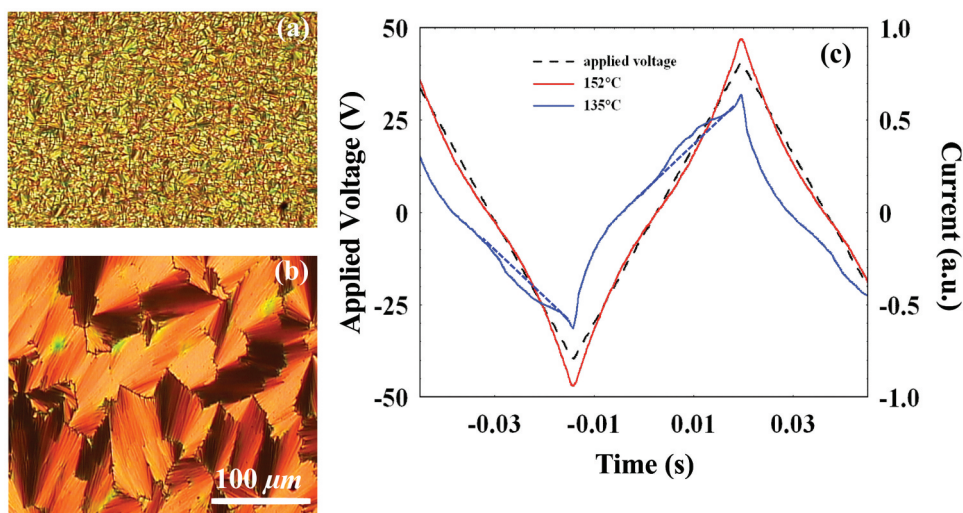


**Figure 4.** (Colour online) Polarisation-switching properties along with POM textures of compound **2** in a 5  $\mu\text{m}$  thick planar with 25  $\text{mm}^2$  area pattern (ITO) at 140°C, before the voltage is applied (a), and after the 16 Hz, 60V<sub>p-p</sub> square wave voltage is applied for 3 minutes (b); (c) Time dependence of electric current under triangular wave voltage. Dashed black line plotted against the left axis is the applied triangular wave voltage. Blue and red lines plotted against the right axis are the electric currents at 135°C (smectic phase) and at 152°C (isotropic phase), respectively. Dotted blue lines are the baselines for the polarisation measurement.

director rotation and backflow-induced domain size increase are characteristic to ferroelectric smectic materials [36]. The increase of the birefringence indicates that the smectic layers are aligned towards the applied field due to the torque between the layer polarisation and the electric field, confirming the ferroelectric nature of the phase. Indeed, polarisation current measurements reveal a ferroelectric type polarisation peak above the steep ohmic baseline. The slope of the baseline indicates a large electric conductivity in the order of  $10^{-7}$  S/m. The area of the peak above the ohmic baseline is  $P_o \sim 100$  nC/cm<sup>2</sup>. This is shown in Figure 4(c), where the time dependence of the electric currents is shown in the smectic phase at 135°C and in the isotropic phase at 152°C under  $U = 60$  V amplitude, 16 Hz triangular wave. In the isotropic phase, the current is basically proportional to the applied voltage indicating only Ohmic origin, while 135°C there is an additional peak indicating polarisation switching. We note that during sign inversion of the applied voltage the optic axis does not rotate, indicating either a SmAP<sub>F</sub> or an anticlinic polar SmC<sub>a</sub>P<sub>F</sub> phase [37].

### 3.2.3 Photoresponsivity

Due to the presence of the stilbene unit in all three materials, one can expect light sensitivity of these materials. For this reason, we performed the UV-Vis absorption spectroscopy on all three compounds in a dichloromethane solution, where we irradiated the materials and placed in quartz tube by 365 nm UV with 1 mW/cm<sup>2</sup> intensity. The results are shown in Figure 4.

The solid lines show the spectra at the initial (dark) state and the dashed lines represent spectra after different times of UV irradiation. In compounds **1** and **3** (Figure 5(a,c)), the absorption at 360 nm decreases at increasing exposure time, but the absorption at lower wavelengths does not change. On the other hand, for compound **2**, while the absorption decreases at 360 nm, it increases at 250 nm. Additionally, a shoulder on the high-energy side of the main absorption band emerges indicating the formation of the *cis*-isomer [38].

The effect of such photoisomerisation of compound **2** was further investigated in 5  $\mu\text{m}$  LC cell under 1 mW/cm<sup>2</sup> intensity, 365 nm wavelength UV illumination. POM images of the textures before, after 15 s and 1 minute UV irradiation at 138°C are shown in Figure 6(a-c), respectively. One can see partial melting to the isotropic phase after 15 s and complete melting after 1 minute of UV illumination. Turning the UV off, the smectic phase did not appear at the constant 138°C even after several hours. Heating to 155°C, above the original clearing point and cooling back, the smectic batonnets started just partially reforming at 138°C (Figure 6(d)), and the phase transition to the smectic phase completed only after cooling to 132°C.

### 3.2.4 Small angle X-ray scattering

In order to verify the nature of the smectic phases of compound **2**, SAXS measurement were carried out and the results are summarised in Figure 6.

In the temperature range above 113°C, the  $q$  dependences of the scattered intensities show two sharp peaks

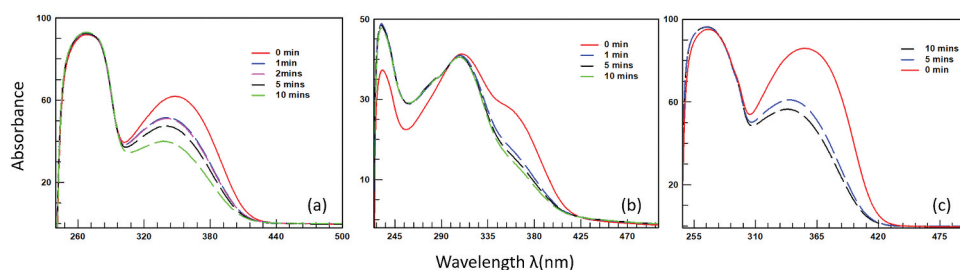


**Figure 5.** (Colour online) UV-Vis absorption spectra of compounds **1**, **2** and **3** in a dichloromethane solution ( $c = 3 \times 10^{-4}$  M) with different illumination time. The solid line represents the isosbestic point, while the dashed lines show the absorbance spectra after different UV exposure times for compounds **1**, **2** and **3**, respectively.

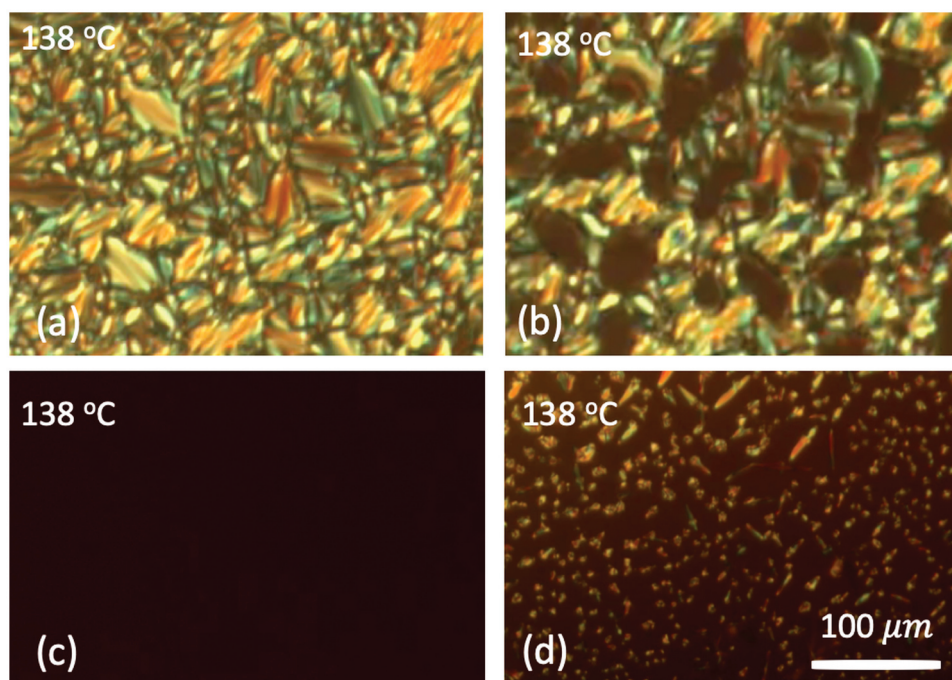


**Figure 6.** (Colour online) POM images of 5  $\mu\text{m}$  thick film of compound **2** at 138°C. (a): texture before UV illumination; (b, c) 15 s and 1 minute after 1  $\text{mW}/\text{cm}^2$  intensity, 365 nm wavelength UV illumination. (d) about 10 minutes after the UV turned off (the sample subsequently heated to 155°C and cooled back to 138°C).

at  $q_1$  and  $2q_1$  (Figure 7(a)). The 2D image shows a slight orientation of the peaks along the magnetic field (Inset of Figure 6(a)). The position of the larger peaks at  $q_1$  varies between  $0.17824 \text{ \AA}^{-1}$  at 144°C and  $0.18647 \text{ \AA}^{-1}$  at 117°C. The  $q$  values correspond to periodicities varying between  $d_1 = (2\pi/q_1) = 35.25 \text{ \AA}$  and  $33.69 \text{ \AA}$ . This 4.4% decrease of the periodicities verifies that the higher temperature polar phase is tilted with increasing tilt angle on cooling. The higher temperature ferroelectric phase therefore can be clearly identified as  $\text{SmC}_a\text{P}_F$  phase. Note, the 1st harmonic at  $q_2 = 2q_1$  is 3 orders of magnitude weaker than the peak at  $q_1$ . From the full width at half maxima (FWHM) the correlation length  $\xi = 1/\text{FWHM}$  of the smectic order is in the range of 300 nm showing well-developed smectic layers with

long-range positional order. With the usual assumption that layer thickness is  $d = l \cos\theta$ , where  $l$  is the molecular length and  $\theta$  is the tilt angle, we can calculate the temperature dependence of the tilt angle in the  $\text{SmC}_a\text{P}_F$  phase as shown by the red dots in Figure 7. Fitting the data with  $\theta(T) = \theta_o + \Delta\theta(T_C - T)^{0.5}$  function corresponding to mean-field theory, we get  $\theta_o = 17^\circ$  and  $\Delta\theta = 1.23$ . Using this fit we find that the molecular length is  $36.87 \text{ \AA}$ , slightly smaller than the fully stretched molecular length  $38.5 \text{ \AA}$  estimated by the software ChemOffice.

In the phase below 113°C, there is a main peak at  $q_1 = 0.17026 \text{ \AA}^{-1}$  with at least 4 harmonics indicating a well-ordered phase. The peak positions are basically independent of the temperature and distinctly smaller than of



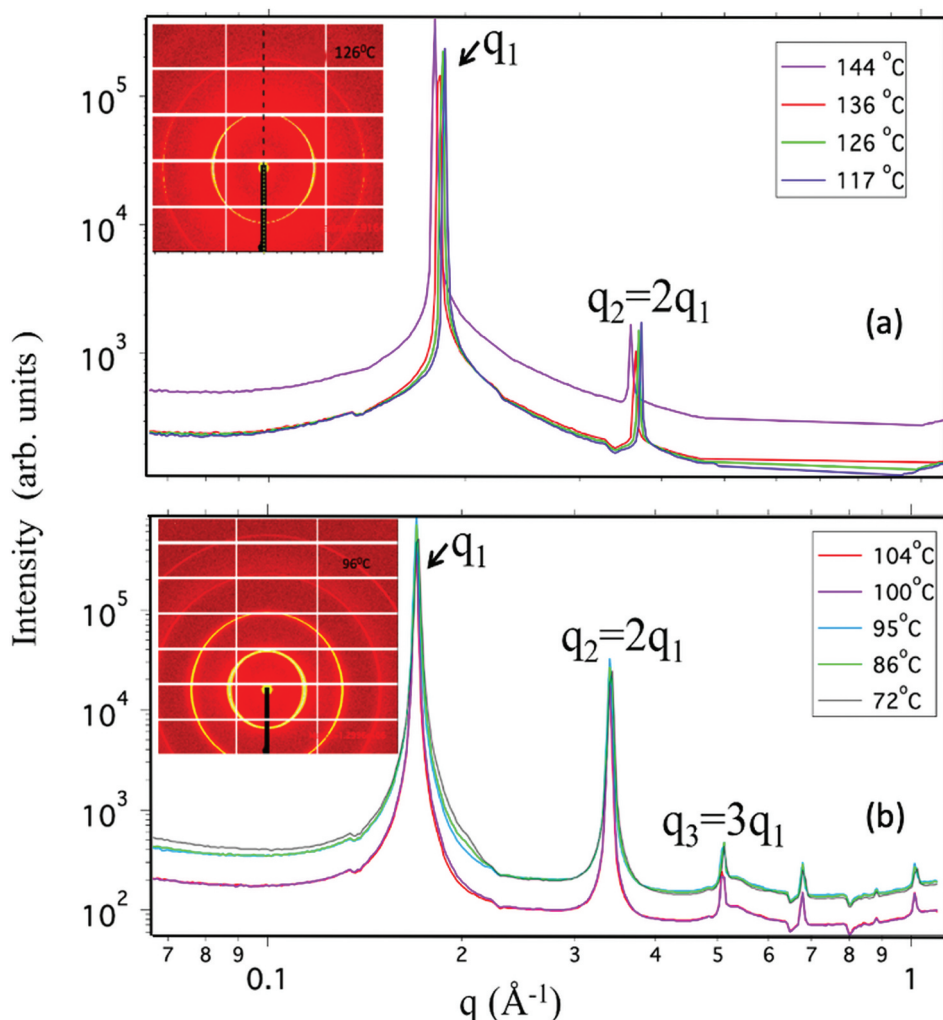


**Figure 7.** (Colour online) Wave number ( $q$ ) dependences of SAXS intensity ( $I$ ) in logarithmic scale in the higher temperature range between 113 °C and 150 °C (a) and in the lower temperature phase below 113 °C (b). Representative 2D SAXS images are in the insets.

the high-temperature phase corresponding to a layer spacing of 36.9 Å (Figure 8). This value is the same that we get for the periodicity at zero tilt angle ( $l$ ). The integer number of SAXS harmonics and the POM textures (see Figure 2(c)) are typical for structures with one-dimensional periodicity, such as smectic phase. However, the abrupt change in the periodicity and the temperature independent periodicity indicate a strong 1st order transition either to a smectic phase with in strong in plane order or to a crystal phase. Due to this ambiguity, we denote this phase as X phase. Combining all the above observations, the proposed phase sequences of compounds 1–3 are listed in Table 1. The mesophases of compounds 1 and 3 are indicated as unknown smectic phase (SmX). Compound 2 has two mesophases and the higher temperature mesophase is identified as SmC<sub>a</sub>P<sub>F</sub> phase. Differential scanning calorimetry (DSC) measurements shown in the Supplementary Information (see Fig. S1) confirm reasonably the proposed phase sequences,

considering the much higher heating/cooling rates applied in the DSC measurements.

#### 4. Conclusions

While investigating the potential of photo-addressable moieties other than azobenzene for design of advanced functional materials, we synthesised and characterised three new bent-core molecules bearing 4-nitrostilbene in a side wing. Results showed that relatively small modifications in the structure of these molecules significantly influenced their supramolecular assembly, which was reflected in formation of various LC phases. Both compound 1 and 3 have an enantiotropic non-polar smectic-type mesophase. Compound 2 with a rigid biphenyl moiety exhibited an SmC<sub>a</sub>P<sub>F</sub> phase, which was replaced by an SmA-type phase at lower temperatures. This material showed UV-induced melting to the isotropic phase so that the original smectic

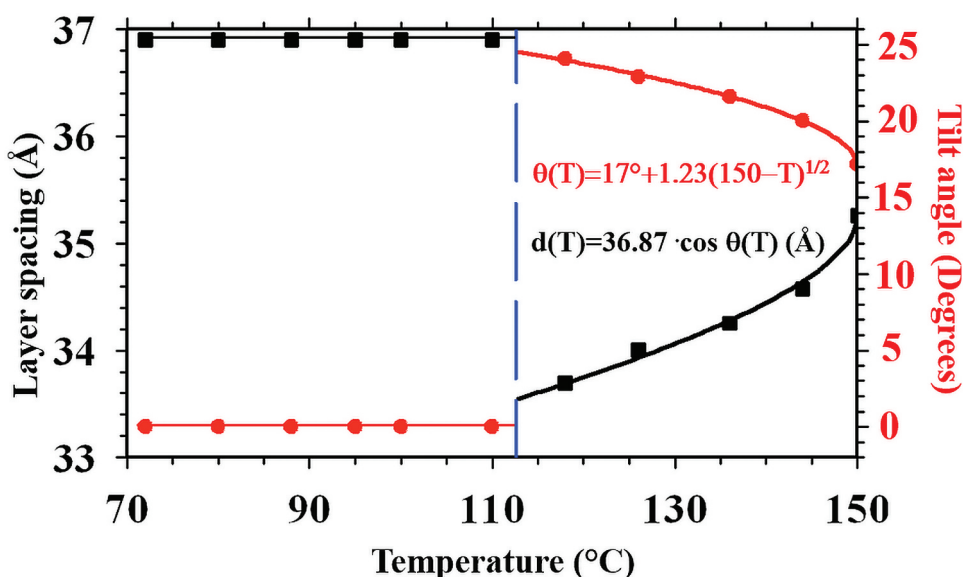


**Figure 8.** (Colour online) Temperature dependences of the measured  $d$  spacing (black solid squares) and the calculated tilt angle (red solid circles). Fitting tilt angle with  $\theta(T) = \theta_0 + \Delta\theta(T_c - T)^{0.5}$  function corresponding to mean-field theory and layer spacing with  $d(T) = l \cos \theta(T)$ .

**Table 1.** Transition temperatures in °C from POM for compounds **1**, **2** and **3**.

Compound	2nd Heating	2nd Cooling
<b>1</b>	Cr 144 SmX 152 I	I 152 SmX 105 Cr
<b>2</b>	X 130 SmC <sub>8</sub> P <sub>F</sub> 150 I	I 150 SmC <sub>8</sub> P <sub>F</sub> 110 X
<b>3</b>	SmX 140 I	I 110 SmX

phase after ceasing the UV irradiation reappeared only at much lower temperatures. This over 10°C drop of the phase transition indicates that the photoresponse of compound **2** driven by polarised light might involve a [2 + 2] cycloaddition reaction leading to the cyclobutane formation, whereby permanent changes were achieved. On the other side, the possibility of decomposition should not be underestimated. This conclusion was supported by the observation of the similar behaviour of structurally related bent-core LCs with a cyanostilbene wing or stilbene-based polymers [30,39]. These characteristics can be applied to obtain materials for optical data storage or UV sensors.

### Acknowledgments

This work was supported by the US. National Science Foundation (NSF) DMR-1904167. The beamline 6.3.3 at the Advanced Light Source at the Lawrence Berkeley National Laboratory is supported by the Director of the Office of Science, Office of Basic Energy Sciences, of the US. Department of Energy under Contract No. DE-AC02-05CH11231. N.T. and L.M. are grateful to the Ministry of Education, Science and Technological Development of the Republic of Serbia for financial support (Contract No. 451-03-68/2020-14/200135; 451-03-68/2020-14/200287). T.T.-K. acknowledges the

financial support from the National Research, Development and Innovation Office (NKFIH) grant no. FK 125134. R.S. and A.J. acknowledge useful discussions and technical help by Dr Chenhui Zhu, Professor Sam Sprunt and Mr Prabesh Gyawali.

### Disclosure statement

No potential conflict of interest was reported by the authors.

### Funding

This work was supported by the US. National Science Foundation (DMR-1904167), the Ministry of Education, Science and Technological Development of the Republic of Serbia (Contract No. 451-03-68/2020-14/200135; 451-03-68/2020-14/200287) and the National Research, Development and Innovation Office of Hungary (NKFIH; grant no. FK 125134).

### References

- [1] Yerushalmi R, Scherz A, van der Boom ME, et al. Stimuli responsive materials: new avenues toward smart organic devices. *J Mater Chem.* 2005;15(42):4480–4487.
- [2] Roy D, Cambre JN, Sumerlin BS. Future perspectives and recent advances in stimuli-responsive materials. *Prog Polym Sci.* 2010;35(1–2):278–301.
- [3] Zhu L, Zhao Y. Cyanostilbene-based intelligent organic optoelectronic materials. *J Mater Chem C.* 2013;1(6):1059–1065.
- [4] Amabilino DB, Smith DK, Steed JW. Supramolecular materials. *Chem Soc Rev.* 2017;46(9):2404–2420.
- [5] Alaasar M. Azobenzene-containing bent-core liquid crystals: an overview. *Liq Cryst.* 2016;43(13–15):2208–2243.

- [6] Kim DY, Jeong KU. Light responsive liquid crystal soft matters: structures, properties, and applications. *Liq Cryst Today*. 2019;28(2):34–45.
- [7] Bieringer T. Photoaddressable polymers. In: Coufal HJ, Psaltis D, Sincerbox GT, editors. *Holographic data storage*. Berlin Heidelberg: Springer-Verlag; 2000. p. p. 209–230.
- [8] Zhou P, Li Y, Li X, et al. Holographic display and storage based on photo-responsive liquid crystals. *Liq Cryst Rev*. 2016;4(2):83–100.
- [9] Jull EIL, Gleeson HF. All-optical responsive azo-doped liquid crystal laser protection filter. *Opt Express*. 2018;26(26):34179–34184.
- [10] Momotake A, Arai T. Photochemistry and photophysics of stilbene dendrimers and related compounds. *J Photochem Photobiol C*. 2004;5(1):1–25.
- [11] Seki T. New strategies and implications for the photoalignment of liquid crystalline polymers. *Polym J*. 2014;46(11):751–768.
- [12] Savyasachi AJ, Kotova O, Shanmugaraju S, et al. Supramolecular chemistry: a toolkit for soft functional materials and organic particles. *Chem*. 2017;3(5):764–811.
- [13] Waldeck DH. Photoisomerization dynamics of stilbenes. *Chem Rev*. 1991;91(3):415–436.
- [14] Lub J, Ferrer A, Larossa C, et al. Synthesis and properties of chiral stilbene diacrylates. *Liq Cryst*. 2003;30(10):1207–1218.
- [15] Fischer T, Ruhmann R, Seeboth A. Photochemically induced structure transfer from analogous azobenzenes and stilbenes onto a liquid crystalline phase. *J Chem Soc Perkin Trans*. 1996;6:1087–1090.
- [16] Ichimura K, Tomita H, Kudo K. Command surfaces 14 [1]. Photoregulation of in-plane alignment of a liquid crystal by the photoisomerization of stilbenes chemisorbed on a substrate silica surface. *Liq Cryst*. 1996;20(4):161–169.
- [17] Ichimura K. Photoalignment of liquid-crystal systems. *Chem Rev*. 2000;100(5):1847–1873.
- [18] Young WR, Aviram A, Cox RJ. Stilbene derivatives. New class of room temperature nematic liquids. *J Am Chem Soc*. 1972;94(11):3976–3981.
- [19] Cox RJ. Liquid crystal properties of methyl substituted stilbenes. *Mol Cryst Liq Cryst*. 1972;19(2):111–122.
- [20] Fouquey C, Lehn JM, Malthête J. Liquid crystals for non-linear optics: mesophases formed by push-pull stilbenes and diacetylenes. *J Chem Soc Chem Commun*. 1987;19:1424–1426.
- [21] Spells DJ, Lindsey C, Dalton LR, et al. Synthesis of terminally substituted stilbene-tolane liquid crystals. *Liq Cryst*. 2002;29(12):1529–1532.
- [22] Ou JC, Hong YL, Yen FS, et al. Cyanated liquid crystals with trans-stilbene structure: syntheses and their cyclo-trimerizations. *J Polym Sci A Polym Chem*. 1995;33(2):313–321.
- [23] Korbecka I, Jaworska J, Galewski Z. Novel fluorescent liquid crystal containing azobenzene and stilbene moieties-synthesis, mesogenic and spectroscopic studies. *Dyes Pigment*. 2017;140:166–168.
- [24] Lehmann M, Hügel M. A perfect match: fullerene guests in star-shaped oligophenylenevinylene mesogens. *Angew Chem Int Ed*. 2015;54(13):4110–4114.
- [25] Lehmann M, Maier P. Shape-persistent, sterically crowded star mesogens: from exceptional columnar dimer stacks to supermesogens. *Angew Chem Int Ed*. 2015;54(33):9710–9714.
- [26] Hügel M, Dechant M, Scheuring N, et al. Fullerene-Filled stilbene stars: the balance between isolated C60 helices and 3D networks in liquid-crystal self-assemblies. *Chem Eur J*. 2019;25(13):3352–3361.
- [27] Gupta RK, Pathak SK, De J, et al. Room temperature columnar liquid crystalline self-assembly of acidochromic, luminescent, star-shaped molecules with cyanovinylene chromophores. *J Mater Chem C*. 2018;6(7):1844–1852.
- [28] Martínez-Abadía M, Varghese S, Milián-Medina B, et al. Bent-core liquid crystalline cyanostilbenes: fluorescence switching and thermochromism. *Phys Chem Chem Phys*. 2015;17(17):11715–11724.
- [29] Martínez-Abadía M, Robles-Hernández B, Villacampa B, et al. Cyanostilbene bent-core molecules: a route to functional materials. *J Mater Chem C*. 2015;3(13):3038–3048.
- [30] Martínez-Abadía M, Robles-Hernández B, de la Fuente MR, et al. Photoresponsive cyanostilbene bent-core liquid crystals as new materials with light-driven modulated polarization. *Adv Mater*. 2016;28(31):6586–6591.
- [31] Pociecha D, Ohta K, Januszko A, et al. Symmetric bent-core mesogens with m-carborane and adamantane as the central units. *J Mater Chem*. 2008;18(25):2978–2982.
- [32] Westphal E, Gallardo H, Sebastian N, et al. Liquid crystalline self-assembly of 2,5-diphenyl-1,3,4-oxadiazole based bent-core molecules and the influence of carbosilane end-groups. *J Mater Chem C*. 2019;7(10):3064–3081.
- [33] Findeisen-Tandel S, Weissflog W, Baumeister U, et al. Laterally substituted symmetric and nonsymmetric salicylideneimine-based bent-core mesogens. *Beilstein J Org Chem*. 2012;8:129–154.
- [34] Martínez-Abadía M, Varghese S, Giménez R, et al. Multiresponsive luminescent dicyanodistyrylbenzenes and their photochemistry in solution and in bulk. *J Mater Chem C*. 2016;4(14):2886–2893.
- [35] Vangala VR, Bhogala BR, Dey A, et al. Correspondence between molecular functionality and crystal structures. Supramolecular chemistry of a family of homologated aminophenols. *J Am Chem Soc*. 2003;125(47):14495–14509.
- [36] Jakli A, Saupe A. Electrically induced uniform planar alignment of SC\* liquid crystals on homeotropically treated plates. *Appl Phys Lett*. 1994;65(22):2777–2779.
- [37] Link DR, Natale G, Shao R, et al. Spontaneous formation of macroscopic chiral domains in a fluid smectic phase of achiral molecules. *Science*. 1997;278(5354):1924–1927.
- [38] Martínez-Abadía M, Varghese S, Romero P, et al. Highly light-sensitive luminescent cyanostilbene flexible dimers. *Adv Optical Mater*. 2017;5(4):1600860.
- [39] Gangadhara KK. Novel photocrosslinkable liquid-crystalline polymers: poly[bis(benzylidene)] esters. *Macromol*. 1993;26(12):2995–3003.